Z. Phys. C – Particles and Fields 34, 91–98 (1987)

Zeitschrift für Physik C Particles and Fields

Expectations of Jet Characteristics at TeV Energies

P.N. Burrows[1] and G. Ingelman[2]

[1] Department of Nuclear Physics, University of Oxford, Oxford, OX1 3RH, UK
[2] Deutsches Elektronen-Synchrotron DESY, Notkestrasse 85, D-2000 Hamburg 52, Federal Republic of Germany

Received 5 November 1986

Abstract. We investigate the properties to be expected of jets produced in future accelerators in the TeV energy domain. Current state-of-the-art models for perturbative jet evolution and non-perturbative fragmentation are used together with experimentally realistic methods for jet reconstruction based on the energy flow pattern in a calorimeter.

1. Introduction

Future accelerator projects in the TeV energy region are presently being investigated in great detail with respect to both the physics potentials and machine aspects [1, 2]. When realised, these accelerators will be abundant sources of high energy jets produced in large momentum transfer processes. Even though jets are interesting in their own right, these costly machines are built rather with the hope to discover new physics phenomena. Many of these will, however, only be observable in terms of jets, e.g. new exotic particles of large masses are expected to decay into quarks and gluons giving rise to high energy jets in the final state. First of all one would therefore like to measure jets and treat them as 'particles', i.e. 4-vectors, to search for new states via resonances in invariant mass combinations of jets. In order to judge how well this can be done and what requirements that the experimental equipment must meet, one needs as detailed information as possible on the properties of jets at this energy scale. The flow of particles and energy within a jet is important for calorimetry and the possibilities to perform tracking in a jet environment and, e.g., to measure special particles like leptons or photons. The concept of a jet is in reality a matter of experimental definition. In order not to give misleading information it is important that the jet properties are obtained using an experimentally realistic jet reconstruction algorithm, rather than being based on theoretical information about unobservable partons.

The purpose of this paper is thus to give the best possible prediction of jet properties at this future energy scale. To this end we employ current knowledge on perturbative jet evolution via the parton radiation processes and the following soft hadronization into observable particles. Both of these processes are simulated using Monte Carlo techniques providing complete events, containing in principle all necessary information. These models have developed significantly within the last few years. They have been tested in detail against data from e^+e^- annihilation at PETRA/PEP energies and are currently being compared to the new jet measurements at the CERN $p\bar{p}$ collider. The generally good ability of the models to reproduce the data gives confidence that the extrapolation to yet higher energies is meaningful. Of course, this extrapolation may turn out to fail once the models can be compared with reality, but this would in itself indicate the occurrence of new physics phenomena.

2. Jet Models

Fixed order perturbation theory has been used to give production properties of jets, e.g. 2^{nd} order QCD in e^+e^- annihilation. However, in order to adequately describe the observed jet characteristics at high energy, multiple gluon emission has also to be taken into account. A general discussion of the ideas involved in such jet models can be found in many papers (see e.g. [3, 4] and references therein) and only the main principles are therefore mentioned here. Partons emerging from a large momentum transfer process, like a hard scattering or the decay of a heavy state, can be off mass shell and thus emit bremsstrahlung partons (mostly gluons) leading to a shower or cas-

cade evolution at the parton level [5, 6]. Monte Carlo techniques are applied to simulate this iterative process which is terminated when the momentum transfer of the parton branching becomes small enough to make perturbation theory unreliable. This is given by the cutoff parameter, t_{cut}, which together with Λ_{QCD} regulates the amount of bremsstrahlung emitted. An interesting sophistication is the possibility to take soft gluon interference effects into account by imposing an angular ordering in the emission [6]. We use such a model as implemented in [7] but also compare with a conventional model without this feature [8] to illustrate the variation of the result due to different models for the QCD cascade evolution.

For the following confinement induced transition of partons into hadrons, one of several alternative non-perturbative models has to be employed. As discussed in [3, 9], the string model [10] is particularly suitable since it provides a desirable stability of the final hadron properties with respect to variations of the arbitrary t_{cut} parameter, and we therefore use this model as the standard case in this study. For comparison, however, we also give some results using the completely different approach of cluster formation and decay [6].

The importance of the parton cascade evolution at high energies has been clearly shown [11] by comparing with jet properties at the CERN $p\bar{p}$ collider measured by the UA1 collaboration [12], but is also needed to reproduce multi-cluster events in e^+e^- annihilation as observed by the JADE collaboration [13] at DESY.

3. Jet Definition

The bremsstrahlung nature of the QCD cascade predominantly results in soft and collinear parton emission, but also occasionally hard emission at large angles resulting in the splitting of a jet into a sub-jet structure. Between these two extremes there is, of course, a continuous distribution which makes the concept of what is a single jet rather arbitrary from the theoretical point of view. More important is the ability to observe experimentally and identify jets. This is usually done from the energy flow pattern in a calorimeter. In order to get realistic results we therefore define a jet using such a method. An idealized 'calorimeter' covers the full azimuthal angle around the beam axis and the pseudo-rapidity region $|\eta| \leq 3$. It is divided into cells of size $\Delta\eta \times \Delta\phi = 0.1 \times 5°$ in each of which the particle energies of a Monte Carlo generated event are summed. Starting from the cell with largest transverse energy, $E_\perp$, the transverse energy of nearby cells within a cone of half-angle

$$\Delta R = \sqrt{\Delta\eta^2 + \Delta\phi^2} \leq 0.7 \quad (1)$$

are summed. If $\Sigma E_\perp$ exceeds a certain cut-off value, E_c, then all the particles within the cone are said to form a jet with axis given by the $E_\perp$-weighted center of the cells. This procedure is iterated until all jets with $E_\perp$ larger than E_c, typically 10–20 GeV, are found.

We have verified that the details of this procedure make no difference to our results by trying the following alternatives: using total energy rather than transverse energy, or taking the initiator cell to define the jet axis. A somewhat different method where each cell is assigned a 4-vector from its energy and position relative to the event vertex, and where the jet vector is obtained by summing the cell 4-vectors also gives essentially the same results, which shows the stability of the properties of these high energy jets with respect to the details of the jet definition algorithm.

We also tried a coarser grained calorimeter, with cell size $\Delta\eta \times \Delta\phi = 0.2 \times 10^0$, and found essentially the same results as those shown below. The longitudinal jet properties stay constant whereas the angular particle and energy flows, Fig. 6, rise somewhat more slowly as θ increases.

The size of the cone used for the jet definition is, however, important for the jet properties since it regulates not only how many soft, wide angle particles that are included in the jet, but also the experimental resolution to separate nearby jets as indicated above. This is shown below by giving results also for the case of a smaller cone with $\Delta R = 0.2$, which is about the smallest possible value for the given calorimeter granularity before fluctuations and leakage between cells become important when only a few cells are used to define a jet.

4. Jets from an e^+e^- Collider

The Lund Monte Carlo [7] is used to generate e^+e^- annihilation events via the electroweak interactions at 2 TeV cms energy. Some results for the LEP/SLC energy of 100 GeV and PETRA/PEP energy of 45 GeV are also given for comparison. Three variations of the perturbative treatment are investigated:

1. coherent QCD cascade including soft gluon interference effects
2. conventional QCD cascade without soft gluon interference effects
3. fixed 2nd order, but exact QCD matrix elements

In all cases the Lund string model is used for the non-perturbative hadronization process. Although

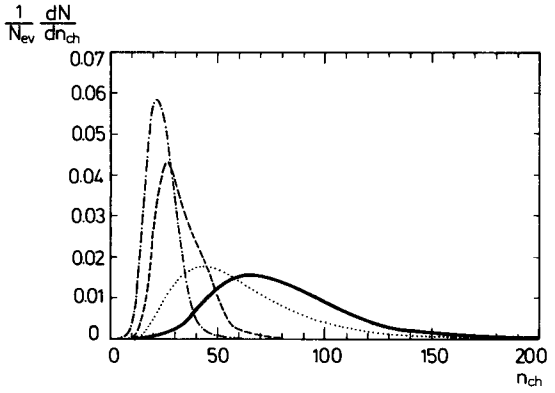

Fig. 1. Charged particle multiplicity distributions for e^+e^- annihilation at 2 TeV cms energy: coherent QCD cascade (full curve), conventional cascade (dotted), 2nd order matrix elements (dashed). Coherent cascade at 100 GeV cms energy (dash-dotted)

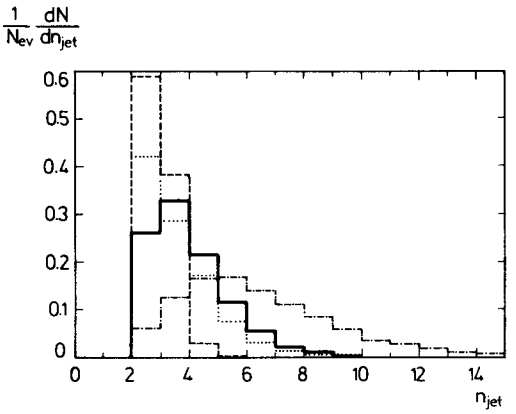

Fig. 2. Number of reconstructed jets per e^+e^- event at 2 TeV (cms). For the standard jet cone size $\Delta R=0.7$: Coherent QCD cascade (full line), conventional cascade (dotted), 2nd order matrix elements (dashed). For the smaller cone $\Delta R=0.2$: coherent cascade (dash-dotted)

the last case is not expected to give realistic jet properties at high energies it is included to illustrate the effects of the multiple gluon emission in the first two cases. Similarly, we believe that the first case is in fact a more sophisticated and satisfactory model than the second.

We also show some results for the model in [6], which incorporates hadronization by cluster formation and decay. We note that all models are tuned to give a satisfactory description of data at present PETRA/PEP energies. In Figs. 1–7 we compare the jet properties resulting from these models. Since each figure thus contains much information through the various curves, we emphasize that it is always the solid line (case 1) which gives our best estimate for the TeV energy jets.

Figure 1 shows the increase of charged particle multiplicity with increased energy and due to multiple gluon emission. The number of jets per event, reconstructed as discussed above with $E_{\perp\text{jet}}>10$ GeV, is given in Fig. 2 and their energy distribution in Fig. 3. The 2nd order QCD model can essentially only give up to four jets whereas with the parton cascade many low energy jets are generated although the rate of high energy jets is roughly the same. The number of jets clearly depends on the size of the cone used to define a jet as seen from the difference between having $\Delta R=0.7$ or 0.2. We note that quark jets dominate over most of the jet energy region, only for $E_{\text{jet}}<300$ GeV do gluon jets become dominant as shown in Fig. 3. (See next section for jet flavour assignment.)

Since the subject of this paper is high energy jets we select for the following study only those jets having E_{jet} within [19, 30], [45, 55] and [900, 1100] GeV from events at cms energies of 45, 100 and 2000 GeV respectively. (Due to the virtuality of an initial quark

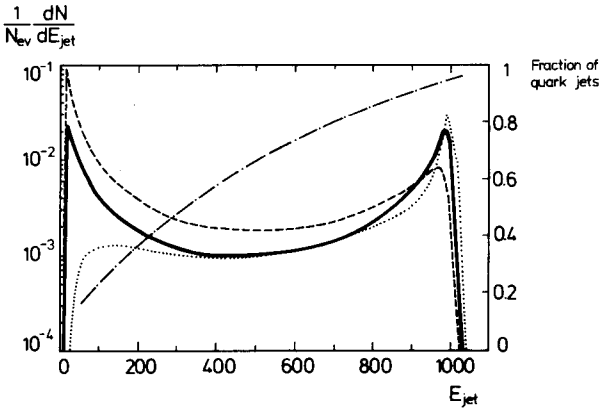

Fig. 3. Energy distribution of reconstructed jets in e^+e^- at 2 TeV (cms) (left hand scale): Coherent QCD cascade (full curve), 2nd order matrix elements (dotted), coherent cascade with $\Delta R=0.2$ (dashed). Dash-dotted curve gives fraction of quark jets (right hand scale), with the jet flavour defined as in Sect. 5

$E_{\text{jet}}>\frac{\sqrt{s}}{2}$ may occur.) The charged multiplicity per jet, obtained as those particles which hit calorimeter cells included in the jet, is given in Fig. 4, and their fragmentation function

$$D^{\text{ch}}(z)=\frac{1}{N_{\text{jets}}}\cdot\frac{dN^{\text{ch}}}{dz} \tag{2}$$

in Fig. 5a. The scaling variable is here chosen as $z=E_{\text{particle}}/E_{\text{jet}}$ after having verified that alternative choices, such as momentum fraction or momentum fraction along the jet axis, give the same results at these energies. A useful quantity is the fraction of all particles which carry energies larger than some minimum value, i.e.

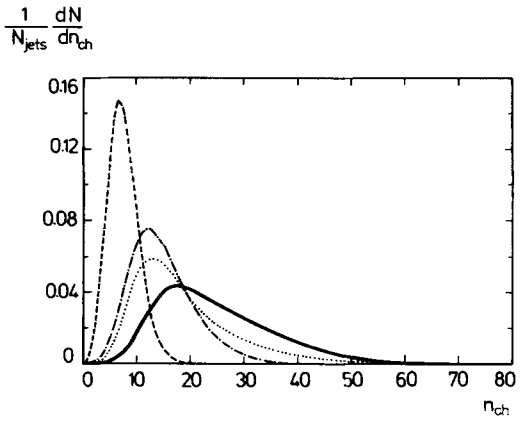

Fig. 4. Charged multiplicity distribution per 'high energy' jet in e^+e^- annihilation. At 2 TeV (cms): coherent QCD cascade (full curve), conventional cascade (dotted), coherent cascade with $\Delta R=0.2$ (dash-dotted). At 100 GeV (cms): coherent cascade (dashed)

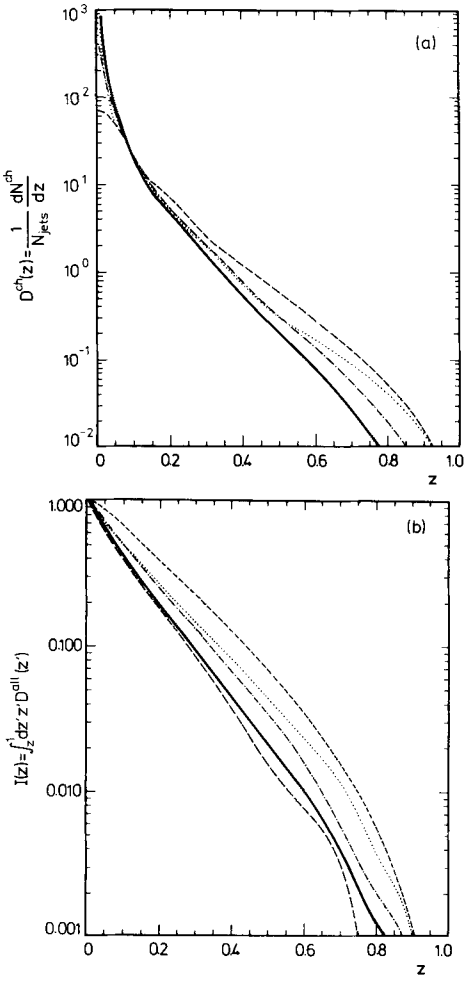

Fig. 5. a Charged particle fragmentation function for 'high energy' jets in e^+e^- annihilation. At 2 TeV (cms): Coherent QCD cascade (full curve), conventional cascade (dotted), coherent cascade with $\Delta R=0.2$ (dash-dotted). At 100 GeV: coherent cascade (dashed). **b** Integral of fragmentation function, (3), for all particles in 'high energy' jets. Curves as in **a**. An additional curve (long dashes) is shown for the coherent QCD cascade model [6] with cluster hadronization at 2 TeV

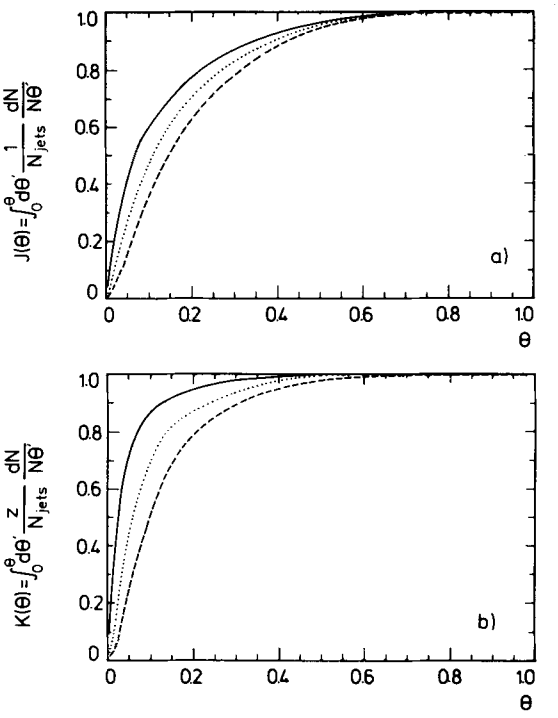

Fig. 6a, b. Integrated angular particle **a** and energy **b** flows (4), (5) resp. for all particles assigned to reconstructed 'high energy' jets in e^+e^- annihilation. Curves are shown for cms energies 2 TeV (full), 100 GeV (dotted), 45 GeV (dashed). Coherent parton cascade and string fragmentation in all cases. (Angle in radians)

$$I(z)=\int_z^1 dz'\,z'\cdot D^{all}(z'), \tag{3}$$

which is shown in Fig. 5b. As an example we note that for 1 TeV jets, 50% (10%) of the jet energy is carried by particles having fractional momentum $z>0.08$ (0.3) corresponding to an absolute energy larger than 80 (300) GeV.

The width of a jet is given in Fig. 6 in terms of the integrated particle and energy flows,

$$J(\theta)=\int_0^\theta d\theta'\cdot\frac{1}{N_{jets}}\cdot\frac{dN}{d\theta'} \tag{4}$$

$$K(\theta)=\int_0^\theta d\theta'\cdot\frac{1}{N_{jets}}\cdot z\cdot\frac{dN}{d\theta'}. \tag{5}$$

Only the results of the coherent cascade are shown here, the conventional cascade gives a similar result and the 2nd order option somewhat narrower jets as expected. Instead, 'high energy' jets within the said energy windows at cms energies of 45, 100 and 2000 GeV are compared to show the narrowing of jets with increasing energy. This is clearly seen, as well as the fact that the energy flow is more collimated than the particle flow. Thus, 50% of the *particles* in

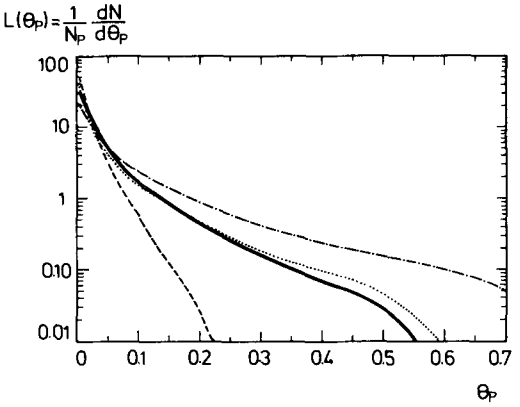

Fig. 7. Distribution of angle between nearest neighbour charged particles, (6), in 'high energy' *jets* in e^+e^-. Curves are for the coherent cascade (full), conventional cascade (dotted), coherent cascade with $\Delta R = 0.2$ (dashed), all at 2 TeV cms energy and string hadronization. (The more rapid fall-off of the latter curve simply reflects the narrower cone definition.) Dash-dotted curve is for all pairs of nearest neighbour charged particles in the *event* for the coherent cascade case. (Angle in radians)

a jet are contained in a cone of half-angle of approximately 8°, 6° and 3° for 45, 100 and 2000 GeV respectively, whereas 50% of the *energy* is within 6°, 3° and 2° respectively.

The separation between particles is important for the possibility to do tracking within a jet and we show in Fig. 7 the angle of each charged particle to its nearest (in terms of angle) neighbour charged particle within the same jet, i.e.

$$L(\theta_p) = \frac{1}{N_p} \cdot \frac{dN}{d\theta_p} \tag{6}$$

normalised to unit area to take into account the different multiplicity in the different cases. (N_p is the total number of charged particles associated to jets in the event sample, i.e. multiplying by $\langle n_{ch}/\text{jet}\rangle$ gives the number of nearest neighbour pairs in a jet.) This distribution is not dominated by low momentum particles; removing all particles with momentum less than 1 GeV has only a small effect.

The conventional model for parton cascade evolution [8], without the angular ordering prescription due to the soft gluon interference effects, is tuned to fit PETRA/PEP data and thus agree well with the coherent model at those energies. Also at $Sp\bar{p}S$ collider energies the two models were found [11] to give very similar results and in fair agreement with UA1 data on jet fragmentation properties [12]. It has also been argued [14] that the coherence effects are within the uncertainty related to the cutoff parameter and too small to be observable experimentally. When extrapolating to TeV energies we find, however, clear differences between the two models as is shown in the figures mentioned above. The conventional parton cascade gives, surprisingly, harder jets with lower particle multiplicity. One would have expected the opposite behaviour since the gluon emission is less restricted without the extra requirement of angular ordering. One should bear in mind, however, that the two cases correspond to completely different program implementations using different methods and making different approximations, e.g. for taking the offshell masses into account in the parton branching process, so that the difference in the effectively available phase space need not be the expected one. The coherent cascade model is theoretically more appealing and it has also been shown to agree better with analytical QCD calculations at extreme energies [15]. We therefore take if as our best estimate and let the differences observed in the conventional model illustrate the theoretical uncertainties involved in the parton cascade approach.

We have also compared the above distributions with those obtained from the model of [6]. The perturbative part is here essentially the same as the coherent case above, but the soft fragmentation differs completely. It is treated by splitting the perturbatively produced gluons at the end of the cascade into quark-antiquark pairs to form colour singlet clusters, which decay into known particles (including resonances) as governed by phase space. A smaller fraction of large mass clusters are, however, split into lighter clusters by a longitudinal string-like decay before the phase space decay is applied. This model is also tuned to data at PETRA/PEP energies. Extrapolating to 2 TeV we find a remarkably good agreement with the Lund model (with coherent cascade) result. This is illustrated in Fig. 5b for the longitudinal jet structure and we note that for the angular energy flow, Fig. 6b, the two models almost coincide (i.e. the full line can well represent both models).

Given this agreement we therefore only consider the coherent Lund model in the following, and give in Table 1 some results on particle multiplicities at

Table 1. Event statistics

	45 GeV	100 GeV	2 TeV
$\langle n \rangle$	34.5	49.0	160
$\langle n_{ch} \rangle$	16.5	23.8	78.3
$\langle n_{ch}/\text{jet} \rangle$	5.5	7.4	24.9
$\langle n_{\pi^\pm} \rangle$	12.2	18.6	63.6
$\langle n_{K^\pm} \rangle$	1.7	2.4	7.4
$\langle n_p \rangle$	0.42	0.62	2.4
$\langle n_\gamma \rangle$	16.5	23.3	77.6
$\langle n_{K^0_L} \rangle$	0.85	1.2	3.5
$\langle n_{e^\pm} \rangle$	0.30	0.42	1.2
$\langle n_{\mu^\pm} \rangle$	0.084	0.17	0.26

different energies. All numbers are per event except those in the third row, which are per high energy jet. It is interesting to note that the average multiplicities obtained by the Monte Carlo agree well, within 10% even at the highest energy, with the expected multiplicity evolution formula derived analytically from leading and next-to-leading order QCD [16] and normalized at low energies to take the uncalculable non-perturbative effects into account.

The fraction of the jet energy carried by charged particles, $\langle E_{ch}/E_{tot}\rangle$, is 0.62 ± 0.01; a quite general result applicable for all studied cms energies and jet energies as well as for the quark and gluon jets of the next section.

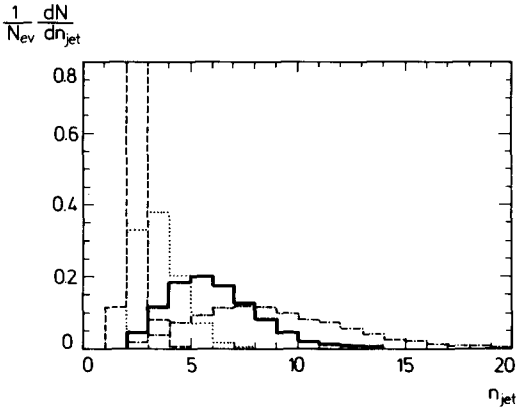

Fig. 8. The number of reconstructed jets per $p\bar{p}$ event at cms energies: 630 GeV (dashed), 2 TeV (dotted), 18 TeV (full), 18 TeV with $\Delta R = 0.2$ (dash-dotted)

5. Jets from a Hadron Collider

Hipp-$p_\perp$ jet events in a $p\bar{p}$ collider are simulated at the three cms energies 0.63, 2 and 18 TeV corresponding to the CERN and Fermilab colliders and a future possible collider in the LEP tunnel [2]. The Lund Monte Carlo [17, 7] based on leading order $2 \to 2$ QCD matrix elements, structure functions [1], coherent final state parton cascade evolution and initial state radiation [18] was used to generate events with a minimum $p_\perp$ of the hard scattering of 30, 100 and 1000 GeV corresponding to $x_\perp \gtrsim 0.1$ at the three cms energies respectively. Higher order QCD matrix elements for $2 \to 3$ and $2 \to 4$ processes have been calculated [19] but the problem of combining them with parton cascade evolution is not solved. As shown by the comparison of fixed order and multiple emission in the previous section, the latter is more important for our purpose of giving the internal properties of a jet.

Using the jet finding algorithm as before, with $E_{\perp\,\mathrm{jet}} > 20$ GeV, which we expect to be enough for the jets to clearly stand out above the underlying event, the expected increase of the jet multiplicities with cms energy is given in Fig. 8. Due to the abundance of gluon jets at a hadron collider we separate the jet properties below into quark and gluon jets. The jet flavour, gluon or quark (q is here q or $\bar{q}$ of any flavour), is obtained from the most energetic parton within the ΔR cone used. An additional requirement of no other parton within the cone of different flavour and energy larger than 70% of the leading parton is also imposed to avoid ambiguous configurations, which are however rather rare. Figs. 9–10 show the longitudinal and transverse properties of quark and gluon jets at the different energy scales. At each energy only high energy jets, E_{jet} within [25, 50], [75, 150] and [750, 1500] GeV, are selected in order to avoid the larger number of low energy jets present due to radiation. (The mentioned $x_\perp$ cutoff also implies that jets below this value will not be free of biases.) Low energy jets can be studied at lower energy accelerators already and are therefore not of primary interest in this context.

Gluon jets are considerably softer than quark jets at all energies, partly due to more perturbative radiation but it is also an important feature of the Lund fragmentation model. For the highest energy jets, Fig. 9b shows that 23% of the quark jet energy is carried by particles having $z > 0.2$ whereas the corresponding number for gluon jets is only $\sim 3\%$. At the lower energies gluon jets are also significantly wider but this difference becomes smaller at the largest energy, presumably due to gluons from the initial quark line being able to generate significant cascading by themselves.

A smaller jet cone, $\Delta R = 0.2$, leads to more low energy jets, Fig. 8, but also a hardening of the high energy jets, Fig. 9b, due to the exclusion of soft, wide angle particles. The angular jet profile is insensitive to the choice of ΔR (not shown) for small angles since the jet core is essentially unchanged, but, of course, the jet energy is saturated at a correspondingly smaller angle (see also Fig. 7).

Since a fully-fledged high-$p_\perp$ hadron collision model based on ref. [6] is not available we cannot directly estimate the model dependent uncertainties of these results as was done for the e^+e^- case above. For quark jets, however, we note that the conclusions obtained in the last section are relevant here also. For gluon jets, we have performed a case study by simulating a gluon-gluon system of invariant mass 2 TeV using the coherent cascade in the program of [6] combined with either its default fragmentation model based on cluster decays or applying the Lund string fragmentation model. We find a generally good

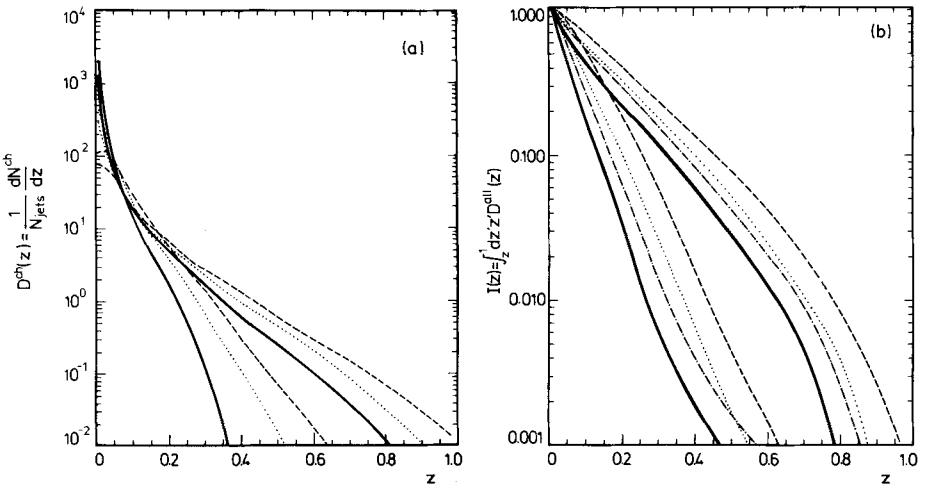

Fig. 9a, b. Fragmentation function **a** and integral of fragmentation function **b** (2), (3) resp. for particles assigned to reconstructed 'high energy' jets in $p\bar{p}$ collisions. Two sets of curves are shown, the energy assignment being the same for each set: cms energies 630 GeV (dashed), 2 TeV (dotted), 18 TeV (full). The harder set is for quark-assigned jets and the softer set for gluon-assigned jets. In **b**, the additional curve (dash-dotted) in each set is for the case 18 TeV cms energy with $\Delta R = 0.2$

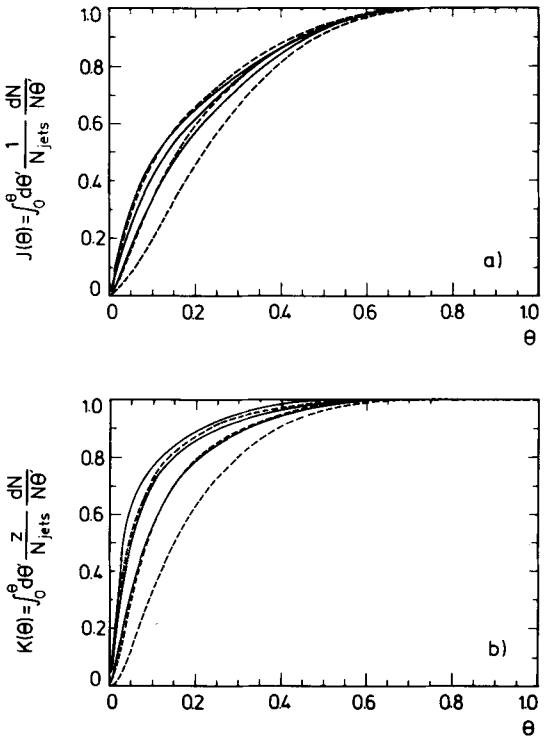

Fig. 10a, b. Integrated angular particle **a** and energy **b** flows within jets (4), (5) resp. for quark jets (full curves) and gluon jets (dashed curves) in $p\bar{p}$. Working towards $\theta = 1$, the curves in each set are for cms energies of 18 TeV, 2 TeV, 630 GeV respectively. (Angle in radians)

agreement between these two fragmentation procedures; the transverse properties of the jets (angular particle and energy flows) are almost identical whereas the cluster model gives a somewhat more steeply falling longitudinal fragmentation function in the large-z region.

6. Conclusion

We note that the 1 TeV quark jets from the hadron collider have very similar properties as those from the e^+e^- annihilation, as expected, since they are produced at comparable Q^2 scales. Since the soft fragmentation is independent of Q^2 and the perturbative scaling violations of the cascade vary as $\ln Q^2$, only small variations with the jet energy and the Q^2 scale are expected. Our results, which are given for particular energy regions, are therefore more general and jets produced at not too different momentum transfers will have essentially the same properties. Since the jet properties examined in this study depend essentially only on the Q^2-scale at which the jets are produced, our results are quite general and not only restricted to the specific jet production mechanisms considered. Thus, jets originating from, e.g., the decay of some high mass state will have very similar properties. It should be noted that a significant part of the jet cross-section in 2 TeV e^+e^- collisons is due to W^+W^- production and decay into quark-antiquark pairs. Since the effective Q^2-scale for the gluon radiation from such quark jets is given by the W mass, these jets will have fragmentation properties similar to those in our study at 100 GeV cms energy (though boosted in the W-direction).

The agreement between the two coherent parton cascade models, [7] and [6], when extrapolated to TeV energies is remarkable since they differ radically in their modelling of the soft fragmentation after the perturbative cascade. Theoretical comparisons between analytical QCD calculations [15] and Monte Carlo simulations give additional support for the reliability of the coherent parton cascade approach and we conclude that there are indeed good reasons to

take the jet characteristics predicted in this study seriously.

Acknowledgements. We are grateful to R. Cashmore and T. Sjöstrand for interesting and helpful discussions.

References

1. E. Eichten, I. Hinchliffe, K. Lane, C. Quigg: Rev. Mod. Phys. **56**, 579 (1984)
2. Proceedings of the ECFA-CERN workshop on 'Large hadron collider in the LEP tunnel', ECFA 84/85 and CERN 84-10
3. G. Ingelman: Phys. Scr. **33**, 39 (1986)
4. T.D. Gottschalk: p. 94 in Supercollider Physics, proceedings of the 1985, Oregon workshop on super high energy physics, Ed. D.E. Soper. Singapore: World Scientific; F. Paige: p. 481 in proceedings of the 1985 international europhysics conference on high-energy physics, Bari, Italy; Ed. L. Nitti, G. Preparata, European Physical Society
5. G.C. Fox, S. Wolfram: Nucl. Phys. **B168**, 285 (1980); R.D. Field, S. Wolfram: Nucl. Phys. **B213**, 65 (1983); T.D. Gottschalk: Nucl. Phys. **B214**, (1983); CALT-68-1083; R. Odorico: Nucl. Phys. **B228**, 381 (1983)
6. G. Marchesini, B.R. Webber: Nucl. Phys. **B238**, 1 (1984); B.R. Webber: Nucl. Phys. **B238**, 492 (1984)
7. T. Sjöstrand: Comp. Phys. Commun. **39**, 347 (1986)
8. We used the conventional cascade implemented in [7] which is based on K. Kajantie, E. Pietarinen: Phys. Lett. **93B**, 269 (1980)
9. T. Sjöstrand: Phys. Lett. **142B**, 420 (1984)
10. B. Andersson, G. Gustafson, G. Ingelman, T. Sjöstrand: Phys. Rep. **97**, 31 (1983)
11. P. Ghez, G. Ingelman: Z. Phys. C – Particles and Fields **33**, 465 (1987)
12. UA1 Collab. G. Arnison et al.: Nucl. Phys. **B276**, 253 (1986)
13. JADE Collab. W. Bartel et al.: DESY preprint 86-086
14. R. Odorico: Z. Phys. C – Particles and Fields **30**, 257 (1986)
15. G. Ingelman, D.E. Soper: Phys. Lett. **148B**, 171 (1984)
16. B.R. Webber: Phys. Lett. **143B**, 501 (1984)
17. H.U. Bengtsson, G. Ingelman, T. Sjöstrand: The Lund Monte Carlo for high-$p_\perp$ scattering, PYTHIA version 4.1, CERN program pool W5045
18. T. Sjöstrand: Phys. Lett. **157B**, 321 (1985)
19. Z. Kunszt, E. Pietarinnen: Nucl. Phys. **B164**, 45 (1980); Phys. Lett. **132B**, 453 (1983); Z. Kunszt, W.J. Stirling: Phys. Lett. **171B**, 307 (1986) (and references therein)